Ab Initio Molecular-Dynamics Simulation of Neuromorphic Computing in Phase-Change Memory Materials

Jonathan M. Skelton,[1†] Desmond Loke,[1,2] Taehoon Lee[1] and Stephen R. Elliott[1]*

[1] Department of Chemistry, University of Cambridge, Lensfield Road, Cambridge, CB2 1EW, UK

[2] Department of Engineering Product Development, Singapore University of Technology and Design, 8 Somapah Road, Singapore 487372, Singapore

Abstract

We present an *in silico* study of the neuromorphic-computing behavior of the prototypical phase-change material, $Ge_2Sb_2Te_5$, using *ab initio* molecular-dynamics simulations. Stepwise changes in structural order in response to temperature pulses of varying length and duration are observed, and a good reproduction of the spike-timing-dependent plasticity observed in nanoelectronic synapses is demonstrated. Short above-melting pulses lead to instantaneous loss of structural and chemical order, followed by delayed partial recovery upon structural relaxation. We also investigate the link between structural order and electrical and optical properties. These results pave the way toward a first-principles understanding of phase-change physics beyond binary switching.

Introduction

The inexorable consumer demand for faster electronic devices is currently being met through the miniaturization of components. However, scaling down existing technologies is rapidly becoming impractical, due to fundamental size constraints imposed by current designs and materials, plus the limitations of lithographic processes.[1] Without increasing the feature density (e.g. number of transistors) in a processing device, performance is set by the effective speed at which the device can perform its various operations.[2] There has thus been a growing interest in alternative computing paradigms, including the co-location of memory and processing (non-von Neumann computing),[3] and hardware implementations of the highly-connected and adaptable neural networks found in nature.[2, 4, 30-34]

The latter brain-inspired ("neuromorphic") computing paradigm is currently one of the most actively explored, and holds much promise for applications requiring large-scale data analyses (so-called "big data"), robotics and intelligent autonomous systems.[5] Traditional processor designs implement a small number of predefined arithmetic and logic operations in hardware, which then form the building blocks for more complex procedures developed in software. In contrast, neuromorphic circuits can automatically optimize the flow of input data through processing elements, implicitly recognizing underlying patterns and constantly evolving a model to adapt to changes over time. By mimicking the dense and highly-connected nature of biological synapses, brain-inspired computing potentially offers an order-of-magnitude improvement in performance and power consumption compared to existing processing technologies.[2]

The key components in neuromorphic circuits are devices which can modulate the strength of connections between other components in response to changing input signals,

mirroring the function of biological synapses. Exposure to an input signal results in temporary changes in synaptic weight which rapidly decay back to the initial value - a behavior termed "short-term plasticity" (STP).[6] Repeated exposure to similar input patterns brings about more permanent weight changes, leading to gradual increases or decreases, termed "long-term potentiation" (LTP) and "long-term depression" (LTD), respectively.[7] This simple set of processes forms the basis of so-called Hebbian learning,[8] a scheme widely used to interpret the response of animal neurons to electrical stimuli (e.g. Ref. [9]). In this model, each synapse receives input from two sources, *viz.* a pre-synaptic and a post-synaptic neuron. Correlated activity spikes on these inputs lead to LTP or LTD, depending on the relative time delay between them, whereas uncorrelated inputs cause only short-lived changes through STP. This relation between signal correlation and the evolution of synaptic weight is referred to as "spike-timing-dependent plasticity" (STDP).[10]

Prototype neural circuits have been demonstrated in the past using a wide variety of electronic switching technologies, including silicon transistors,[5] memristors,[2] and, more recently, resistive[11] and phase-change random-access memory (PCRAM) devices.[4] PCRAM seems to be a particularly good candidate,[30] as it naturally exhibits the switching characteristics required for a reconfigurable interconnect through the fundamental nature of its operation. PCRAM is typically implemented as a binary memory, with digital information being encoded in the structure of a phase-change material (PCM), by switching it rapidly and reversibly between (meta)stable amorphous and crystalline phases with large contrasts in electrical resistance and/or optical reflectivity. However, both the amorphization and crystallization processes are analogue in nature, and so with careful selection of writing-current pulses, progressive changes in the

conductivity of a PCRAM cell can be effected, allowing it to function as an electronic synapse whose strength can be modulated with high precision.

PCRAM is also a scalable technology, which is essential for practical array-level neuromorphic computing, where scalability and energy consumption are both important considerations. In this regard, PCRAM boasts a number of highly-desirable features, including a simple device structure, low power consumption, fast switching speed, and small feature size.[12] Synaptic operations requiring energies in the picojoule range have been achieved with PCM cells,[4, 31, 32] while complete devices requiring <1 mW of power in operation have also been demonstrated.[33] The main limitation on energy consumption is the (re)amorphization process, which requires a large energy input to melt a microscopic region of the cell by Joule heating, although this can be optimized in aggressively-scaled devices.[24, 31]

Neuromorphic computing using PCM-based devices has been demonstrated by several groups. Suri *et al.* designed a neural network based on two PCM elements per synapse, in which the crystallinity, and hence conductivity, of one element contributes a negative weight to the output current, while the state of the other contributes positively.[33] By avoiding the use of amorphization pulses in modulating the conductivity, the device power requirements were limited to a very low level. The authors were able to train their system to detect objects within images with a high success rate. A subsequent adaptation showed that a programming scheme based on binary switching could be used in place of "multilevel" analogue conductivity variation,[34] simplifying device design and improving reliability. A prototype PCM chip that acts like a brain network of 913 neurons with 1,650,000 synapses between them has also been demonstrated by researchers at IBM.[13]

Kuzum and coworkers have similarly demonstrated a device which mimics the Hebbian learning seen experimentally in rat neurons.[4, 9] In their implementation, a partially-crystalline starting state receives a steady stream of "pre-spike" pulses together with a variable "post-spike" pulse, representing inputs from two connected neurons. The pre-spikes come in two sets: one set are pulses which heat the PCM above its crystallization temperature, but whose duration is too short to induce significant structural ordering, while the second set are longer pulses which heat to below the crystallization temperature. If a post-spike overlaps with a pre-spike, the combined heating effect is sufficient to induce melt-quenching (former pulse set) or crystallization (latter pulse set), thereby decreasing or increasing the conductivity of the connection (depressing/ potentiating), respectively. The pre-spikes can be arranged in a staircase fashion, so that different post-spike timings lead to different degrees of conductivity change, and hence adjusting the amplitude, length and spacing of the input pulses allows the electronic synapse to display different characteristic responses to its inputs.

In this work, we model *in silico* the behavior of a prototypical PCM in a neuromorphic-computing scenario using *ab initio* molecular-dynamics (AIMD) simulations. Such first-principles simulations have been shown to be a valuable tool in characterizing the microscopic behavior of PCMs during memory operation,[15, 16, 18, 19] and thus could provide valuable information to complement ongoing research on their application in neuromorphic circuits. Whereas these simulations are presently limited to relatively small systems of ~100s of atoms (e.g. [25, 26]) the use of quantum-mechanical calculations avoids the complexities of parameterizing (semi-)empirical force fields to reproduce the subtleties of the local structure of the elements in multicomponent PCM systems, and the behavior through the phase change, which is a complex task.[35] We chose to model the scheme reported by Kuzum *et al*.,[4] since the synaptic device

therein is based on a single PCM cell, and makes use of both amorphization and crystallization pulses to effect conductivity modulation, allowing us to investigate the feasibility of modeling both in our simulations.

Our results show that a reasonable representation of spike-timing dependent plasticity can be achieved in AIMD simulations, with stepwise changes in the material structural order being observed in response to multiple thermal stimuli of different time durations and amplitudes. Structural ring-based and chemical-order analyses reveal the phase-change kinetics in the PCM and the microscopic changes in material order harnessed in neuromorphic-computing synaptic elements. We also model the effect of changes in structural order on the electrical and optical properties of our models.

Methods

We have performed AIMD simulations using the Vienna *Ab initio* Simulation Package (VASP) code.[14] 180-atom models were created in cubic supercells, with periodic boundary conditions, at a fixed density of 6.11 g cm^{-3}. These constant-volume conditions were chosen to mimic the effectively constant-volume setup of typical PCM "sandwich" device structures; the density is the typical value used in AIMD simulations on GST,[15-19] and is intermediate between the experimentally-measured amorphous and crystalline densities. We employed PAW pseudopotentials,[20] treating the outer *s* and *p* electrons as valence electrons, in conjunction with the Perdew-Burke-Enzerhof (PBE) exchange-correlation functional[21] and a plane-wave kinetic-energy cut-off of 175 eV. The Brillouin zone was sampled at the Gamma point. The temperature in the MD simulations was controlled using a Berendsen thermostat,[22] and a timestep of 5 fs was used to propagate the dynamics.

For more detailed electronic-structure and optical-property calculations, the structures obtained from the MD simulations were used without ionic relaxation. The plane-wave cut-off was increased to 500 eV in these calculations, and a denser 4x4x4 Gamma-centered Monkhorst-Pack **k**-point mesh[36] was used for Brillouin-zone sampling. The number of bands was also increased to 1728 (triple the default) to ensure the convergence of the sum over empty states when calculating the optical properties using the linear-response routines in VASP.

We prepared an initial starting configuration for the neuromorphic-computing simulations as follows. An amorphous structure was generated by a melt-quench procedure similar to that typically used in other PCM simulations.[15-17] An initial starting configuration was randomized at 3000 K for 20 ps, then equilibrated as a liquid at 1200 K for 40 ps. An amorphous model was then obtained by quenching to 300 K at a cooling rate of $\mathrm{d}T/\mathrm{d}t = -15$ K ps^{-1}. We partially crystallized the amorphous model by annealing it at 500 K for 500 ps, which was sufficient for the number of fourfold rings in the model, a representative measure of structural order, to stabilize. Further simulations were then carried out on this final configuration, as described in the text.

We quantified the structural order in our models by the number of fourfold rings, the building block of the metastable cubic crystal (rocksalt) form of GST, present. Fourfold rings were defined, as in Refs. 14, 15, by four atoms forming a closed path with a maximum bonding distance (here 3.5 Å), and with all four three-atom bond angles, plus the angle between the planes defined by two triplets of atoms, being a maximum of 20° from the ideal angles of 90° and 180°, respectively. As in e.g. Refs. 14, 17, we quantified the chemical order in our models in terms of the atomic bonding. An ideal rocksalt structure contains only Ge/Sb-Te heteropolar bonds, and thus could be viewed as being composed solely of $[Ge,Sb]_2Te_2$ fourfold rings. We

therefore classified the rings in our model based on their atomic composition, and the class of chemically-ordered rings in this definition would exclude those containing homopolar Ge-Ge, Sb-Sb and Te-Te bonds, as well as heteropolar Ge-Sb bonding.

Results and Discussion

We developed a temperature-pulse sequence to mimic *in silico* the STDP behavior emulated by the PCM-based devices reported by Kuzum *et al.*[4] (Figure 1). The pre-spike base sequence for the depression consists of a staircase arrangement of 5 ps temperature pulses of 600, 610 and 635 K, interspersed with 40 ps rest periods at 300 K. These pulses were found to be of sufficient amplitude, but too short in duration, to induce significant crystallization. Three additional simulations were then performed to mimic post-spike pulses coincident with each of the three pre-spikes, modeled by increasing each of the pulse temperatures by 300 K to 900, 910 and 935 K, respectively (Figure 1c). These pre/post-spike combinations heat the model above the experimental melting temperature of GST of around 900 K[15]. For the potentiation simulation, the pre-spike sequence consists of a train of 50 ps pulses at 375, 335 and 310 K, again interspersed by 40 ps rest periods. These pulses are of sufficient length, but have too low an amplitude, to induce crystal growth; however, in an analogous manner to the depression sequence, coincident post-spike pulses of 300 K boost these heat pulses above the crystallization temperature of the material.

Figures 1 d, e show the change in the number of fourfold rings in the model at the end of the sequence, averaged over the last 20 ps of the final rest period, relative to the value obtained from the base sequence with no post-spikes. As noted, these plots illustrate that the two pulse sequences yield a reasonable representation of the STDP characteristics of the device in Ref. [4].

As expected, post-spike pulses overlapping with different pre-spikes in the depression sequence lead to a reduction in the number of rings at the end of the simulation, reducing the degree of crystallinity in the model, which would in turn lead to a decrease in conductivity (e.g. by increasing the size of the amorphous regions separating crystallites). On the other hand, a post-spike overlapping with a potentiation pulse gives rise to a growth in structural order, indicative of an increase in conductivity. There is a sharp fall-off in the (dis)ordering effect as the post-spike occurs further away from the last pulse in the depression sequence or the first in the potentiation simulation, respectively, marking another characteristic of Kuzum *et al.*'s device, and of the biological system it was designed to emulate.[9]

To investigate the effect of the degree of structural order in the initial state on the device behavior, and to verify our results on the partially-crystalline model using an alternative starting configuration, we further performed a depression simulation on an amorphous starting model, generated by annealing the as-quenched amorphous model at 300 K for 150 ps until the number of fourfold rings stabilized (see supporting information). We were able to reproduce a similar behavior to that shown in Figure 1 using one of the sequences we tested; however, in contrast to the simulations on the partially-crystalline model, the difference in the number of rings resulting from different post-spike timings was somewhat smaller, to the point that conductivity changes may not be noticeable in a working device.

In the scheme modeled in this work, the key parameters controlling the response characteristics of the neuromorphic synapse are the pulse length and temperature. The effects of various single pulse lengths and amplitudes on the structural order in our partially-crystalline model were therefore independently investigated (Figure 2). We found that the low-temperature annealing of the melt-quenched amorphous model prior to the neuromorphic simulations led to

the formation of a small stable crystalline cluster (Figure 2c, top), which could subsequently be grown proportionately in response to heat pulses of varying amplitude and duration (Figures 2a, b).

For this model, the operating range for the pulse length was found empirically to be 5-50 ps. We note that this is a much shorter timescale than the nanosecond pulses typically employed in current PCM-based devices,[23] which we attribute to the much smaller size of our model, plus possibly discrepancies between the temperatures used in our simulations and the effective temperatures induced by Joule heating from the low-voltage pulses applied in PCM-based neuromorphic devices.[4] On the other hand, switching at aggressively-scaled device sizes[24] and on sub-nanosecond timescales[25] have both been demonstrated experimentally, and thus we interpret these pulse lengths as being a possible lower bound for the speed of operation of optimized devices, i.e. nanoscale PCM-based devices driven by ultrafast electrical (or laser) excitations.

When applying a sequence of 50 ps heat pulses with progressively-increasing temperatures between 500 and 700 K (spanning the typical AIMD crystallization temperature of around 600 K[15]), the number of fourfold rings in the model increases with each pulse, and in proportion to the pulse amplitude. A similar phenomenon is observed when 700 K pulses with successively longer lengths are applied, although it can be seen that the induced structural ordering is rather more asymmetric with respect to pulse length, with the shorter pulses having relatively little effect on the structural order. Strikingly, these simulations suggest that the crystal growth may occur via a two-stage step-like process, whereby the heat pulse initially causes a reduction in the number of rings, followed by reformation of these ordered units and a subsequent growth, which occur both during the application of the pulse and at the beginning of the subsequent rest period at 300 K. It is worth noting, however, that the thermostat employed in

the simulations does not allow for temperature fluctuations, and this, in combination with the temperature being increased instantaneously on application of the heat pulses, rather than being ramped, may exaggerate the initial decrease in the ring count.

While the atomistic processes occurring during the melt-quenching and crystallization of GST have been studied extensively,[15, 16, 18, 26] melting and annealing simulations are typically performed with the system held at a fixed temperature, and with the simulations being run until completion. It is therefore of interest to characterize the temporal changes in structural and chemical order which occur during the simulated potentiation and depression sequences, in order to establish whether the material physics underpinning the progressive switching - in particular on the picosecond timescales and at the small length scales being explored in the present work - are different to those which underlie binary switching. Figure 3 shows the time evolution of the number of fourfold rings in our model during the four simulations in the depression sequence, together with the fraction of rings containing only Ge/Sb-Te bonds (i.e. no "wrong bonds"), which acts as a measure of the chemical order in the system.[18]

During the pre-spike sequence, without additional overlapping post-spike pulses, the number of fourfold rings in the model increases slightly following the second and third pulses, indicating that these background pulses are capable of inducing small structural changes. There is a concomitant small increase in chemical order, which suggests that the changes are due to structural relaxation, e.g. the annealing out of bonding defects formed during the rapid quenching, which were not removed during the pre-annealing treatment.

As expected, all three pre/post-spike combination pulses lead to a large and sharp reduction in the ring count, equal to roughly 50 % of the base value; the magnitude increases with the amplitude of the pulse, but the difference is small, mirroring the relatively small

temperature differences between them. In contrast, however, the chemical disordering induced by the three pulses differs significantly, such that the three pre/post-spike combinations lead to quite different levels of chemical disorder. Strikingly, in the simulations where the post-spike overlaps with the first and second pre-spikes, significant structural relaxation occurs when subsequent pre-spike pulses are applied, leading to a regrowth of rings and a corresponding chemical ordering - this effect appears to make an important contribution to the differences in ring counts at the end of the four simulations (i.e. the final synaptic weight).

A similar analysis of the potentiation sequence (see supporting information) shows that, in this part of the simulation, the dominant effect is simply the growth of structural order in response to the crystallization pulses; although the pulses do lead to a small dynamic disordering, the effect is much smaller than in the depression simulations, and it occurs only when the pulse is first applied, and is completely reversed by the beginning of the following rest period.

A previous study of the melting kinetics in GST[17] proposed a melting mechanism in which a crystalline cluster first fragments into disconnected medium-range-ordered structural units, *viz.* planes and cubes of atoms, which subsequently break up into discrete fourfold rings, which themselves finally dissolve as the system melts. Based upon the present results, this can be extended to the progressive melting modeled in the depression sequence. Heat pulses above the melting temperature induce a 'thermal shock' in the material, breaking bonds and forming a significant concentration of defects (e.g. dangling bonds), most likely at the crystal-glass interface. The rapid quenching following the pulse leads to this disordered state being 'frozen in'. Provided the disordered structures are metastable, insufficient thermal energy is available during the rest phases to facilitate the atomic diffusion required to remove them, at least not on a short timescale, whereas the short bursts of energy delivered by subsequent pre-spike pulses can

lead to a delayed reordering. This appears to be mediated initially by the annihilation of chemically-disordered ('frustrated') structural units, which spontaneously reform as ordered entities, and perhaps then act as an attachment site for additional atoms.

This mechanism provides a natural explanation for the fact that we found the structural ordering in our model depended quite sensitively on the amplitudes of the pulses in the pre-spike sequence in the depression part of the simulation (see supporting information). We found it necessary to employ a significant amount of trial and error in order to obtain a sequence which mimicked the behavior of the device reported by Kuzum *et al.*,[4] with the major difficulty being selecting pre-spike temperatures which did not induce significant structural ordering in isolation, but caused appreciable disordering when boosted by a post-spike pulse, and which, when boosted, also limited regrowth during the following rest period, and following other pre-spike pulses later in the sequence. Based on these results, then, the selection of pre- and post-spike heat-pulse sequences for depression represents a balance between inducing a measurable disordering in a short time when the two overlap, while simultaneously controlling the structural relaxation and delayed reordering which can arise from isolated pre-spike pulses.

We stress again that these considerations will be most important in the regime of small device sizes and very short pulses. For longer pulse times and larger devices, it is reasonable to assume that the material may reach a (microscopic) equilibrium during the application of the heat pulses, which would minimize the effect of delayed reordering on the electrical characteristics. Moreover, we note that the difficulties which we experienced in selecting suitable pulse sequences most likely indicate that the size of our model may be close to the lower limit of what is appropriate for these simulations. Size effects would be much less prominent in larger systems, and the effect of model size on the behavior in simulations such as those in the present study may

represent important follow-up work - particularly if longer or more intricate pulse sequences are to be analyzed using similar methods. Despite these limitations, the present findings provide useful insight into the physics of ultrafast operation in nanoscale neuromorphic phase-change devices, and suggest that, as devices are scaled down, the operating window for the selection of suitable pulses to mimic a particular STDP response may narrow.

In the present work, our focus has been on characterizing the structure of the models, with the degree of structural and chemical order being taken as a marker of the electrical/optical characteristics of the material. To confirm this relation, we computed electronic density of states (DoS) curves for each of the final configurations obtained at the end of the depression and potentiation sequences shown in Fig. 1, together with the optical reflectance, R, as a function of wavelength, both at the PBE level of theory. Fig. 4 shows the DoS near the Fermi energy, E_F, of the two sets of models, along with the percentage change in reflectance relative to the respective reference sequences consisting of only pre-spike pulses.

Both sets of DoS curves exhibit the commonly-encountered problem with (semi-)local DFT exchange-correlation functionals, *viz.* the absence of a clear energy gap between the valence and conduction states.[37] It is difficult to identify any systematic trends among the depression-sequence curves. Sequences "B" and "C", which lead to the largest degradation of structural order with respect to the reference sequence ("A"), appear to reduce the density of states near E_F, which could reflect a drop in conductivity. However, the variation among all four sequences is subtle, which most likely indicates that the changes in structural order produced during the depression sequences do not have a large impact on the bulk electronic structure of the material. Among the crystallization sequences, sequence "T", which leads to a significant structural ordering, appears to lead to a correspondingly marked shift in the valence and

conduction-band edges to higher energies, which is suggestive of a possible increase in conductivity due to the enhanced crystallinity. Sequences "U" and "V", which lead to relatively little change in structural order with respect to the reference simulation, lead to rather less marked changes in the respective DoS curves.

Similar phenomena are broadly evident in the reflectance curves. Comparing Figs. 1 (d) and 4 (c), a reduction in the ring count with respect to the reference model appears to lead to fairly small changes in reflectance, at least when set against the changes which occur as a result of the potentiation sequences, which is consistent with the similarly small changes in the DoS. On the other hand, according to the results in Fig. 4 (d) the growth of the ordered cluster during potentiation leads to a decrease in reflectivity in the wavelength range between ~150-300 nm, and an increase from 300-800 nm. Interestingly, when compared against Fig. 1 (e), the ordering of the reflectivity changes is consistent with the changes in structural order which result from the three potentiation sequences with overlapping post spikes.

For completeness, calculated electrical-conductivity tensors, obtained from a semi-classical model for band transport, are given in the supporting information. However, for reasons discussed therein, accurate modeling of the electrical conductivity remains a significant challenge to first-principles calculations at present, and as a result of these limitations, the results are unlikely to be reliable, and we therefore do not discuss them here.

Finally, two other questions of significant interest are those of the number of discrete resistance states achievable in ultra-scaled PCM cells, and also the stochasticity of the switching process. Although we have not sought specifically to investigate the former in this study, from a structural-order perspective, the results presented in Fig. 2 suggest that ~4 discrete levels between a partially-crystalline starting state and a fully-crystalline final state could be achieved

through crystallization pulses. In principle, additional resistance levels could be achieved through amorphization, but the difficulties we experienced in optimizing the pulse sequences for this purpose, and the apparently lower contrast between different levels of amorphization with respect to a partially-crystalline reference state, suggest that this may be more difficult to control. Having only performed a limited number of simulations of our chosen pulse sequence, we do not have sufficient statistics to investigate quantitatively the stochasticity of the switching. Indeed, the difficulty of repeating simulations a large number of times represents one of the current limitations of AIMD modeling in general. We were able to obtain similar qualitative structural-ordering behavior in depression simulations starting from both a partially-crystalline and an amorphous model (c.f. Fig. 1; see also Fig. S5), which suggests that the characteristic response of an ultra-scaled synapse could be reliably reproduced against variation in the initial state of the PCM, whereas the absolute values of e.g. the conductivity may be more variable. Stochasticity of switching may therefore become an increasingly important issue as devices are scaled down, and is something which merits further investigation.

Conclusion

In summary, we have modeled *in silico* the response of the prototypical phase-change material, GST, to a pulsed time-temperature profile, which is key to its application to PCM-based neuromorphic computing. A very good demonstration of spike-timing dependent plasticity was achieved, with a stepwise increase in the material order in response to multiple heat pulses of different lengths and heights. Structural and chemical-order analyses reveal the phase-change kinetics in GST and the microscopic changes in material order which are harnessed in synaptic elements. We have also established a link between the degree of structural order in the materials

and the resulting variation in electronic and optical properties, although further work on calculating these properties more accurately is required. This study could provide a pathway for the development of neuromorphic-computing simulation tools which can readily identify suitable next-generation PCMs and rapidly optimize state-of-the-art device performance. Moreover, the demonstration that first-principles calculations and simulations can potentially be used to study the response of a material to intricate temperature variations suggests that similar methods to those employed here might be used to investigate related phenomena, e.g. the arithmetic and logic devices demonstrated experimentally in other studies.[3, 27, 28]

Figures
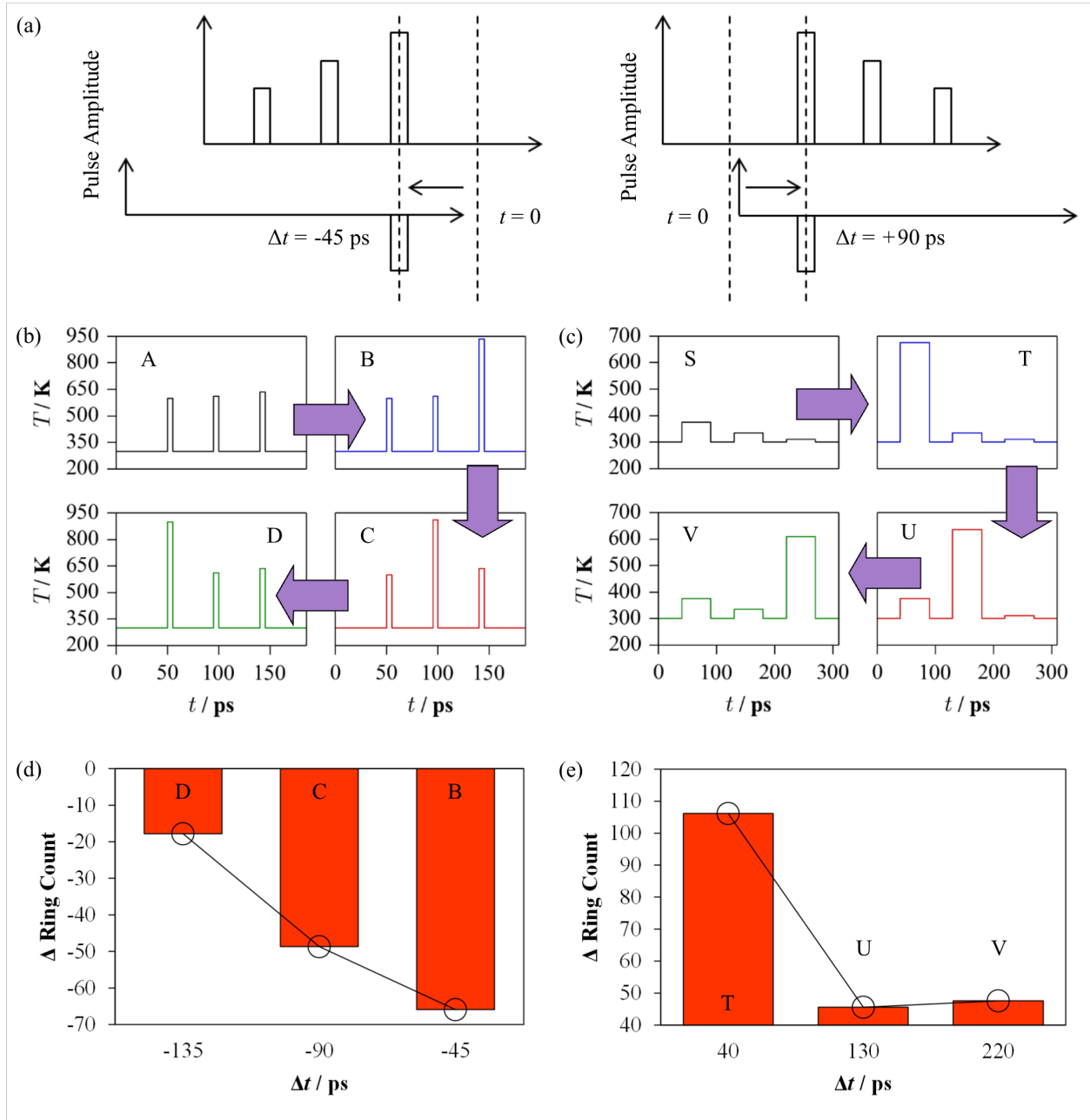
Figure 1. *In silico* emulation of spike-timing-dependent plasticity (STDP) in a partially-crystalline model of Ge$_2$Sb$_2$Te$_5$. The schematic in (a) illustrates the process adopted for the simulations of depression (left) and potentiation (right); in both, a post-spike pulse overlapping with one of a sequence of pre-spikes yields a combined pulse temperature which depends on the

post-spike timing. Plots (b) and (c) show the depression and potentiation heat-pulse sequences, respectively, adopted to mimic the STDP behavior modeled by the device reported by Kuzum *et al.*[4] Within each regime, four simulations were performed (marked A-D and S-V in (b) and (c), respectively): in the first, the material is subject to only the staircase of pre-spike pulses (A/S), while in the other three, a coincident post-spike pulse boosts one of the three pre-spikes by 300 K (B-D/T-V). Plots (d) and (e) show the change in the number of fourfold rings in the model at the end of the sequence, averaged over the last 20 ps of the final rest period, relative to the value obtained from the pre-spike sequence with no overlapping post-spikes. The decay in the (dis)ordering effect as the post-spike occurs further from the time zero (the end of the depression and start of the potentiation, respectively) is a feature of the rat neurons studied by Bi and Poo,[9] which was incorporated into the neuromorphic circuit developed in Ref. [4].
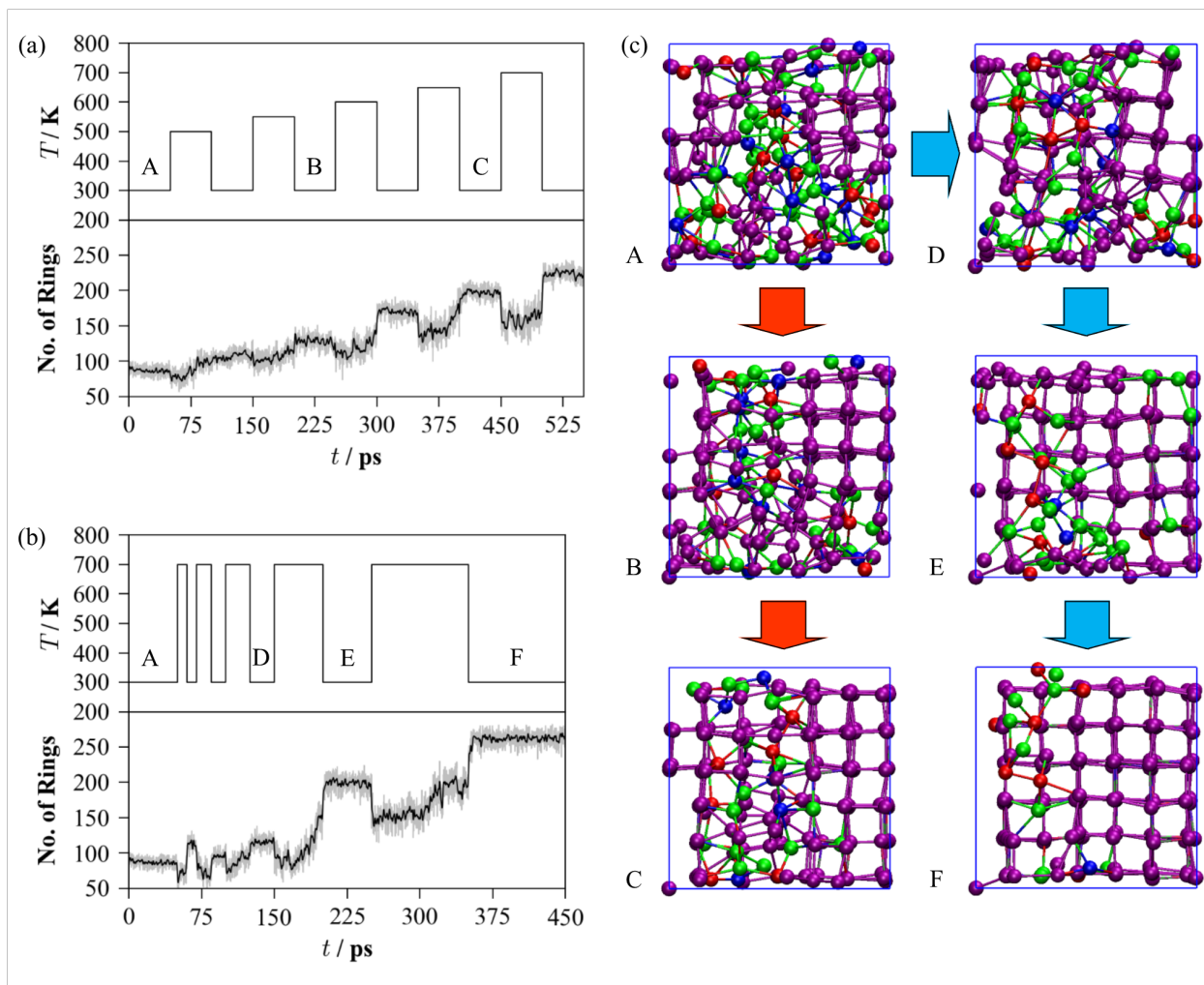
Figure 2. Heat-pulse-induced structural ordering in a simulated partially-crystalline model of $Ge_2Sb_2Te_5$. Plot (a) shows the effect of a sequence of 50 ps temperature pulses with successively larger amplitudes (top) on the number of fourfold rings present in the model (bottom). Plot (b) has the same layout, and shows the effect of varying the temperature-pulse duration with a fixed amplitude of 700 K. The snapshots of the model in (c) are taken from the middle of the rest periods marked A, B and C in plot (a), and A, D, E and F in plot (b), and show the progressive growth of an initially small crystalline cluster. Atoms forming parts of fourfold rings are colored purple, and the color coding of the other atoms is as follows: Ge - blue, Sb - red, Te - green. These snapshots were prepared using the VMD software.[29]
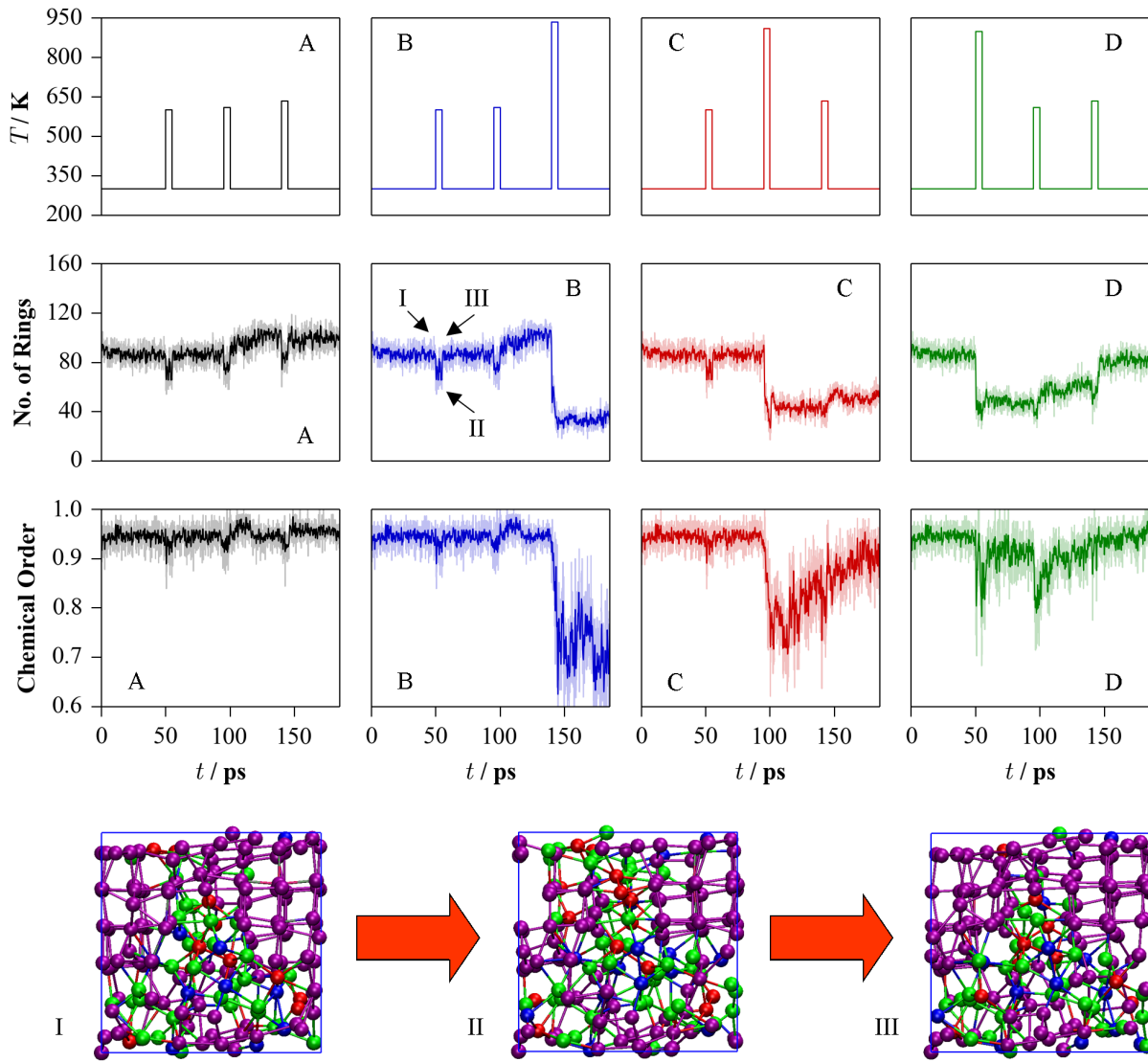
Figure 3. Evolution of the structural and chemical order in a model of $Ge_2Sb_2Te_5$ during a simulated depression heat-pulse sequence. The top row of plots shows the temperature-time profiles of the four parts of the simulation, modeling (from left to right): the pre-spike sequence with no overlapping post-spike (A), and the same sequence with post-spike pulses coincident with the first (B), second (C) and third (D) pre-spikes. The second row shows the corresponding time evolution of the number of fourfold rings in the model, which is an indication of the level of structural order. The bottom row of plots shows the fraction of the rings which contain only chemically-correct Ge/Sb-Te bonds, employed here as a measure of the degree of chemical order

in the model. Snapshots from sequence B at the time points marked I, II and III, taken before, during and after a pre-spike, respectively, are shown at the bottom of the figure, and illustrate the dynamic disordering induced by the pulse. The color coding of the atoms in these snapshots is as in Figure 2, and the images were prepared using VMD.[29]
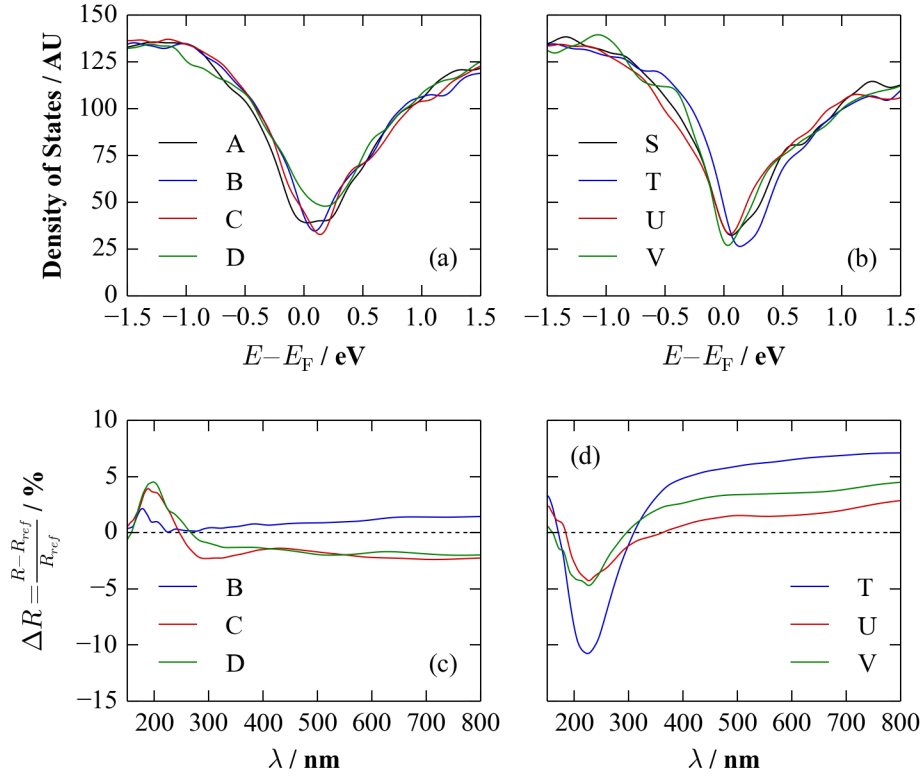
Figure 4 Electronic structure and optical properties of the final configurations of the models obtained from the depression (a, c) and potentiation (b, d) pulse sequences shown in Fig. 1, calculated at the PBE level of theory. The labeling and line colors have been chosen to be consistent with those in Fig. 1. Plots (a) and (b) compare the electronic densities of states near the Fermi energy (E_F), while plots (c) and (d) compare the simulated reflectance as a function of wavelength, expressed relative to that of the reference configuration with only the background pre-spike pulse sequence applied to it (labeled A and S in the depression and potentiation sequences, respectively).

Supporting Information. Includes data from the various pulse sequences tested during the optimization of the depression and potentiation sequences discussed in the text, an analogous figure to Fig. 3 for the potentiation simulation, data from a depression simulation on an amorphous starting model, and the calculated conductivity tensors to accompany the data in Fig. 4. The Supporting 553 Information is available free of charge on the ACS Publications website at DOI: 10.1021/acsami.5b01825.

Data-Access Statement. The key raw data discussed in this manuscript is available online free of charge from http://dx.doi.org/10.15125/BATH-00098. All other data discussed in the article and supporting information is available from the authors on request.

Corresponding Author

*E-mail: sre1@cam.ac.uk

Present Addresses

†Department of Chemistry, University of Bath, Claverton Down, Bath, BA2 7AY, UK

Author Contributions

JMS and DL designed the project. JMS carried out the simulations, and JMS, DL and THL analyzed and interpreted the results. JMS and DL drafted the publication, and all authors contributed to proof-reading and correcting the draft. SRE supervised the project. All authors have given their approval of the final version of the manuscript.

References

1. Lu, W.; Lieber, C. M. Nanoelectronics from the Bottom Up. *Nat. Mater.* **2007**, *6*, 841-850.

2. Jo, S. H.; Chang, T.; Ebong, I.; Bhadviya, B. B.; Mazumder, P.; Lu, W. Nanoscale Memristor Device as Synapse in Neuromorphic Systems. *Nano Lett.* **2010**, *10*, 1297-1301.

3. Wright, C. D.; Hosseini, P.; Vazquez Diosdado, J. A. Beyond Von-Neumann Computing with Nanoscale Phase-Change Memory Devices. *Adv. Funct. Mater.* **2013**, *23*, 2248-2254.

4. Kuzum, D.; Jeyasingh, R. G. D.; Lee, B.; Wong, H. S. P. Nanoelectronic Programmable Synapses Based on Phase Change Materials for Brain-Inspired Computing. *Nano Lett.* **2012**, *12*, 2179-2186.

5. Rachmuth, G.; Shouval, H. Z.; Bear, M. F.; Poon, C. S. A Biophysically-Based Neuromorphic Model of Spike Rate- and Timing-Dependent Plasticity. *Proc. Natl. Acad. Sci. U. S. A.* **2011**, *108*, E1266-E1274.

6. Zucker, R. S. Short-Term Synaptic Plasticity. *Annu. Rev. Neurosci.* **1989**, *12*, 13-31.

7. Caporale, N.; Dan, Y. *Annu. Rev. Neurosci.*; Annual Reviews: Palo Alto, CA, **2008**; pp 25-46.

8. Hebb, D. O. *The Organization of Behavior: A Neuropsychological Theory*; Wiley: New York, **1949**.

9. Bi, G. Q.; Poo, M. M. Synaptic Modifications in Cultured Hippocampal Neurons: Dependence on Spike Timing, Synaptic Strength, and Postsynaptic Cell Type. *J. Neurosci.* **1998**, *18*, 10464-10472.

10. Markram, H.; Lubke, J.; Frotscher, M.; Sakmann, B. Regulation of Synaptic Efficacy by Coincidence of Postsynaptic APs and EPSPs. *Science* **1997**, *275*, 213-215.

11. Yu, S. M.; Gao, B.; Fang, Z.; Yu, H. Y.; Kang, J. F.; Wong, H. S. P. A Low Energy Oxide-Based Electronic Synaptic Device for Neuromorphic Visual Systems with Tolerance to Device Variation. *Adv. Mater.* **2013**, *25*, 1774-1779.

12. Wuttig, M. Phase-Change Materials - Towards a Universal Memory? *Nat. Mater.* **2005**, *4*, 265-266.

13. Burr, G.; Shelby, R.; di Nolfo, C.; Jang, J.; Shenoy, R.; Narayanan, P.; Virwani, K.; Giacometti, E.; Kurdi, B.; Hwang, H. Experimental Demonstration and Tolerancing of a Large-Scale Neural Network (165,000 Synapses), Using Phase-Change Memory as the Synaptic Weight Element. *IEEE Int. Electron Dev. Meet.* **2014**, 29.5.1-19.5.4.

14. Kresse, G.; Hafner, J. Ab Initio Molecular Dynamics for Liquid Metals. *Phys. Rev. B* **1993**, *47*, 558(R).

15. Hegedus, J.; Elliott, S. R. Microscopic Origin of the Fast Crystallization Ability of Ge-Sb-Te Phase-Change Memory Materials. *Nat. Mater.* **2008**, *7*, 399-405.

16. Lee, T. H.; Elliott, S. R. Ab Initio Computer Simulation of the Early Stages of Crystallization: Application to $Ge_2Sb_2Te_5$ Phase-Change Materials. *Phys. Rev. Lett.* **2011**, *107*, 145702.

17. Loke, D.; Skelton, J. M.; Law, L. T.; Wang, W. J.; Li, M. H.; Song, W. D.; Lee, T. H.; Elliott, S. R. Guest-Cage Atomic Interactions in a Clathrate-Based Phase-Change Material. *Adv. Mater.* **2014**, *26*, 1725-1730.

18. Skelton, J. M.; Loke, D.; Lee, T. H.; Elliott, S. R. Structural Insights into the Formation and Evolution of Amorphous Phase-Change Materials. *Phys. Status Solidi B* **2013**, *250*, 968-975.

19. Skelton, J. M.; Loke, D.; Lee, T. H.; Elliott, S. R. Understanding the Multistate SET Process in Ge-Sb-Te-Based Phase-Change Memory. *J. Appl. Phys.* **2012**, *112*, 064901.

20. Blochl, P. E. Projector Augmented-Wave Method. *Phys. Rev. B* **1994**, *50*, 17953-17979.

21. Perdew, J. P.; Burke, K.; Ernzerhof, M. Generalized Gradient Approximation Made Simple. *Phys. Rev. Lett.* **1996**, *77*, 3865-3868.

22. Berendsen, H. J. C.; Postma, J. P. M.; Vangunsteren, W. F.; Dinola, A.; Haak, J. R. Molecular-Dynamics with Coupling to an External Bath. *J. Chem. Phys.* **1984**, *81*, 3684-3690.

23. Bruns, G.; Merkelbach, P.; Schlockermann, C.; Salinga, M.; Wuttig, M.; Happ, T. D.; Philipp, J. B.; Kund, M. Nanosecond Switching in GeTe Phase Change Memory Cells. *Appl. Phys. Lett.* **2009**, *95*, 043108.

24. Feng, X.; Liao, A. D.; Estrada, D.; Pop, E. Low-Power Switching of Phase-Change Materials with Carbon Nanotube Electrodes. *Science* **2011**, *332*, 568-570.

25. Loke, D.; Lee, T. H.; Wang, W. J.; Shi, L. P.; Zhao, R.; Yeo, Y. C.; Chong, T. C.; Elliott, S. R. Breaking the Speed Limits of Phase-Change Memory. *Science* **2012**, *336*, 1566-1569.

26. Kalikka, J.; Akola, J.; Larrucea, J.; Jones, R. O. Nucleus-Driven Crystallization of Amorphous $Ge_2Sb_2Te_5$: A Density Functional Study. *Phys. Rev. B* **2012**, *86*, 144113.

27. Cassinerio, M.; Ciocchini, N.; Ielmini, D. Logic Computation in Phase Change Materials by Threshold and Memory Switching. *Adv. Mater.* **2013**, *25*, 5975-5980.

28. Loke, D.; Skelton, J. M.; Wang, W.-J.; Lee, T. H.; Zhao, R.; Chong, T.-C.; Elliott, S. R. Ultrafast Phase-Change Logic Device Driven by Melting Processes. *Proc. Natl. Acad. Sci. U. S. A.* **2014**, *111*, 3272-13277.

29. Humphrey, W.; Dalke, A.; Schulten, K. VMD: Visual Molecular Dynamics. *J. Mol. Graphics* **1996**, *14*, 33-38.

30. Suri, M.; DeSalvo, B. Phase Change Memory and Chalcogenide Materials for Neuromorphic Applications: Emphasis on Synaptic Plasticity. In *Advances in Neuromorphic Memristor Science and Applications*; Kozma, R. Pino, R., Pazienza, G., Eds.; Springer: Dordrecht, 2012; Vol. 4, Part 2, pp 155-178.

31. Kuzum, D.; Jeyasingh, R. G. D.; Wong, H.-S. P. Energy Efficient Programming of Nanoelectronic Synaptic Devices for Large-Scale Implementation of Associative and Temporal Sequence Learning *IEEE Int. Electron Dev. Meet.* **2011**, 30.3.1-30.3.4.

32. Kuzum, D., Jeyasingh, R. G. D.; Shimeng, Y.; Wong, H.-S. P. Low-Energy Robust Neuromorphic Computation Using Synaptic Devices. *IEE Trans. Electron Device* **2012**, 3489-3494.

33. Suri, M.; Bichler, O.; Querlioz, D.; Cueto, O.; Perniola, L.; Sousa, V.; Vuillaume, D.; Gamrat, C.; DeSalvo, B. Phase Change Memory as Synapse for Ultra-Dense Neuromorphic Systems: Application to Complex Visual Pattern Extraction. *IEEE Int. Electron Dev. Meet.* **2011**, 4.4.1-4.4.4.

34. Garbin, D.; Suri, M.; Bichler, O.; Querlioz, D.; Gamrat, C.; DeSalvo, B. Probabilistic Neuromorphic System Using Binary Phase-Change Memory (PCM) Synapses: Detailed Power Consumption Analysis. *IEEE Int. Conf. Nanotechnol.* **2013**, 91-94.

35. Sosso, G. C.; Miceli, G.; Caravati, S.; Behler, J.; Bernasconi, M. Neural Network Interatomic Potential for the Phase Change Material GeTe. *Phys. Rev. B* **2012**, *85*, 174103.

36. Monkhorst, H. J.; Pack, J. D. Special Points for Brillouin-Zone Integrations. *Phys. Rev. B* **1976**, *13*, 5188.

37. Seidl, A.; Vogl, G. P.; Majewski, J. A.; Levy, M. Generalized Kohn-Sham Schemes and the Band-Gap Problem. *Phys. Rev. B* **1996**, *53*, 3764.

Table of Contents Graphic